Effect of Microstructure on Creep Crack Growth Behavior of a Near-α Titanium Alloy IMI-834

D.V.V. SATYANARAYANA, C.M. OMPRAKASH, T. SRIDHAR, and VIKAS KUMAR

In the present study, the effect of microstructure (*i.e.*, $\alpha + \beta$ and transformed β) on creep crack growth (CCG) behavior of a near-alpha (IMI 834) titanium alloy has been explored at temperatures 550 °C and 600 °C. For characterizing the CCG behavior of the alloy, both stress intensity factor (K) and energy integral parameter (C_t) were used in the present investigation. The use of stress intensity factor (K) as crack-tip parameter is not appropriate in the present study as no unique correlation between crack growth rate and K could be obtained from the observed trend due to transients in the creep crack rate data. On the other hand, C_t parameter for both microstructural conditions consolidates CCG data into a single trend. The alloy with fully transformed β microstructure exhibits better CCG resistance as compared to bimodal ($\alpha + \beta$) microstructure. This is consistent with the fact that the transformed β structure offers superior creep resistance as compared to $\alpha + \beta$ microstructure. Microstructural examination has revealed that CCG for both microstructural conditions is accompanied by formation of damage zone in the form of numerous environmental-assisted secondary surface cracks (perpendicular to the stress axis) ahead of the main crack tip. For $\alpha + \beta$ microstructure of the alloy, the surface creep cracks were formed by growth and coalescence of microcracks nucleated by fracture of primary α particles. While in the interior of the specimens, CCG occurred by growth and coalescence of microvoids nucleated at primary α/transformed β (matrix) interfaces. For β microstructure of the alloy, while the surface creep cracks formed by growth and coalescence of microvoids nucleated at titanium enriched surface oxide particles, in the interior CCG occurred by nucleation of intergranular cavities.

DOI: 10.1007/s11661-008-9684-1
© The Minerals, Metals & Materials Society and ASM International 2008

I. INTRODUCTION

THE aeroengine components operating at high temperatures are prone to creep failure due to high sustained rotational speeds. Also, the components during service are frequently subjected to varying stresses and temperatures and thus become susceptible to localized creep or fatigue damage, which leads to initiation of cracks early in life. As a result, a significant portion of component life may be spent in crack growth stage. Under such conditions, fracture mechanics-based damage tolerance design codes are being recommended for design and life management of aeroengine components. The implementation of these codes requires crack growth characterization of materials under near service loading conditions. Well-established fracture mechanics-based crack growth models, in the form of Paris equation, are available to account fatigue loading at ambient temperatures. At elevated temperatures, the stress intensity factor, K, based on linear elastic fracture mechanics (LEFM) concepts is found to be inappropriate for characterization of fatigue crack growth behavior of materials to account for the effect of superimposed dwell periods as typically encountered in aeroengine service loading cycles. This is because during dwell periods damage due to creep also becomes significant and contributes to overall damage.[1] Under such conditions, path-independent energy integrals C^* or C_t based on elastic plastic fracture mechanics (EPFM) concepts as recommended by ASTM E-1457 standard[2,3] have been used to characterize creep crack growth (CCG) behavior of materials. Extensive work on CCG behavior of power plant steels[4–10] and aeroengine materials, such as nickel-based superalloys,[11,12] has been reported in literature. However, similar studies on titanium-based alloys are very limited,[13–15] in particular, with regard to microstructural aspects of CCG micromechanisms.

High-temperature near-α titanium alloys are extensively used for compressor components of aeroengines due to their excellent high-temperature specific strength with good combination of creep and fatigue properties. During the last decade, there has been thrust to develop near-α titanium alloys containing Al, Zr, Sn, Mo, and Nb with small amount of Si. The IMI-834 is one of the latest near-α alloys developed for compressor discs, blades, and vanes of modern aeroengines. Though there have been several efforts to understand effect of microstructure on creep micromechanisms of this alloy, CCG behavior of the alloy has not been reported in literature. However, a few studies on other titanium alloys

D.V.V. SATYANARAYANA, C.M. OMPRAKASH, and VIKAS KUMAR, Scientists, are with Defense Metallurgical Research Laboratory, Kanchanbagh, Hyderabad-500058, India. Contact e-mail: dvvsn@rediffmail.com T. SRIDHAR, Team Leader, is with National Institute of Technology (NIT), Warangal 560004, India.

Manuscript submitted April 17, 2008.
Article published online October 24, 2008

characterizing the CCG behavior using various crack-tip parameters (K, J, C^*, or C_t) depending on their creep-brittle or creep-ductile nature, have been reported.[13–15] Further, unlike nickel-based superalloys, the effect of microstructure on CCG mechanisms in titanium alloy is not well understood. Therefore, the objectives of the present study on IMI-834 titanium alloy include (1) to investigate the effect of microstructure, namely, bimodal ($\alpha + \beta$) and fully transformed β, on CCG behavior at two temperatures in near-service range, (2) to explore suitable crack-tip parameter (K or C_t) to uniquely characterize CCG behavior, and (3) to understand CCG micromechanisms.

II. EXPERIMENTAL PROCEDURE

A. *Material*

The chemical composition of the studied alloy in weight percent is Ti-5.8Al-3.0Sn-3.33Zr-0.38Nb-0.32Mo-0.33Si. The alloy used in the present investigation was supplied in the standard thermomechanically treated condition (bimodal microstructure, *i.e.*, $\alpha + \beta$) in the form of an 18-mm-diameter rod used for compressor blade application. In order to study the alloy with fully transformed β structure, a β treatment consisting of heating the alloy into the β range at 1075 °C (β transus ~1025 °C) for 0.5 hour followed by air cooling, and aging at 700 °C for 2 hours, was given. The CCG behavior of the alloy for both of these microstructural conditions, *i.e.*, $\alpha + \beta$ and fully transformed β, was investigated. The optical micrograph shown in Figure 1(a) illustrates microstructure of the alloy in as-received condition, *i.e.*, ($\alpha + \beta$) treated condition, which exhibits ~15 pct volume fraction of primary α within transformed β matrix. The primary α is in equiaxed form with an average size of ~40 μm as determined by the linear intercept method. The transformed β is in lath form with an average lath size ~10-μm thick. The average prior β grain size in bimodal microstructure is ~250 μm. The optical micrograph (Figure 1(b)) of the alloy in the β treated condition reveals the presence of only transformed β with an average lath size ~7-μm thick. The average prior β grain size for β treated condition is higher, *i.e.*, ~350 μm, as compared to that in bimodal microstructure as solution temperature (1075 °C) in the former case being higher.

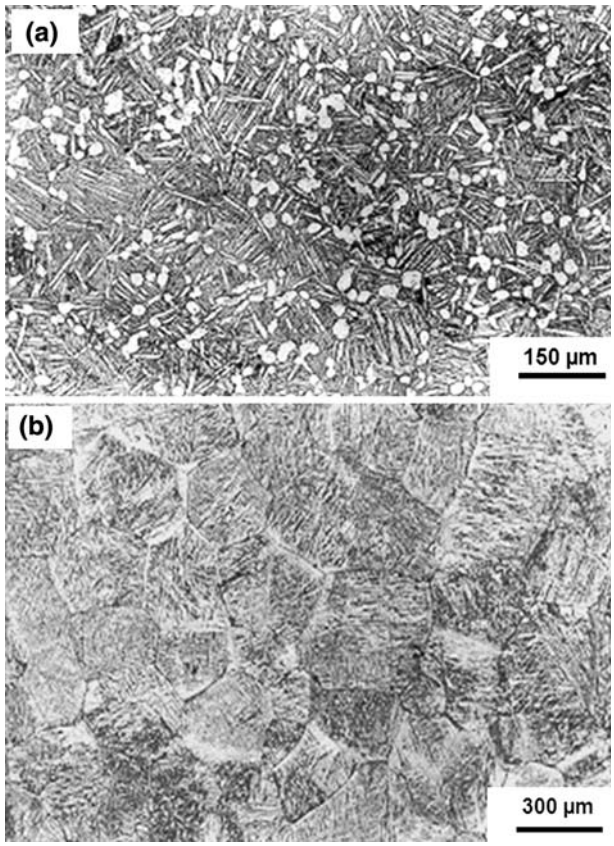

Fig. 1—Microstructure of IMI-834 titanium alloy (*a*) $\alpha + \beta$ and (*b*) β treated condition.

B. *CCG Characterization*

Creep crack growth testing was performed at two temperatures, 550 °C and 600 °C. As per ASTM E-1457 standard,[2] the compact tension (CT) type geometry specimen has been recommended for CCG tests. Since the material used in the investigation was in 18-mm rod form, single edge notch tension (SENT) type specimen geometry having width of 15 mm, thickness of 2 mm, and gage length of 40 mm was adopted. A straight notch of 1-mm depth and 0.1-mm radius was cut in the specimen by using electro discharge machining wire cut machine. Prior to testing, gage portion of samples were polished metallographically and lines were engraved at an interval of 0.5 mm to measure crack length optically during CCG testing. The specimens were precracked at a stress ratio of 0.1 at room temperature by using a high-frequency resonance fatigue testing machine. The maximum load used for precracking was kept less than the load employed for the CCG testing (usually maintained around 50 pct of the CCG test load). A constant load lever arm-type CCG testing frame with a lever ratio of 1:10 was used in the present investigation. The furnace has a quartz glass window on the front door for viewing the specimen for monitoring the crack growth optically during CCG studies. The crack growth was continuously recorded using alternating current potential drop (ACPD) technique. A constant current of 2 A was passed through the specimen using platinum wires spot welded to the specimen. The voltage drop across the crack mouth was measured using another set of platinum wires spot welded to the specimen. The load line displacement (LLD) was measured by using linear variable differential transformer (LVDT) extensometers with an accuracy of ± 1 μm. Both the output values of ACPD and LVDT were continuously recorded during the test at a regular interval of time by a data acquisition system. Tests were continued until the fracture of specimens. A few tests were interrupted several times to measure crack length for calibration as well as to examine damage evolution ahead of the crack tip.

C. *Data Analysis*

The data analysis has been performed using various crack-tip parameters K, C_t, and C^* as described extensively in literature.[2–16] The stress intensity factor K for SENT-type of specimen is calculated using the formula[17]

$$\Delta K = f(\alpha)\sigma\sqrt{\pi a} \quad [1]$$

where $f(\alpha)$ is defined as

$$f(\alpha) = 1.12 - 0.231\alpha + 10.55\alpha^2 - 21.72\alpha^3 + 30.39\alpha^4 \quad [2]$$

where α is the ratio of crack length to width of the sample, *i.e.*, (a/W), σ the applied stress, and a the crack length. In order to characterize crack growth behavior under a wide range of conditions from small scale creep (SSC) to extensive steady-state creep regime, C_t parameter, as proposed by Saxena,[16] is more appropriate and it can be calculated from experimental data using expression of the form

$$C_t = (C_t)_{SSC} + C^* \quad [3]$$

where

$$(C_t)_{SSC} = (1 + (t_T/t))C^* \quad [4]$$

$$t_T = K^2(1-\upsilon^2)/(E(n+1)C^*) \quad [5]$$

$$C^* = P\upsilon'_{SS}(n-1)/(2BW(1-a/w)(n+1)) \quad [6]$$

where t_T[18,19] is the transition time (*i.e.*, the time when the small scale stress fields equal the extensive steady-state stress fields characterized by C^*), υ the Poisson's ratio, n the stress exponent, E the elastic modulus, and $\acute{\upsilon}_{SS}$ steady-state LLD rate. Further, since the creep zone is a damaged region surrounding the crack tip as shown subsequently, the additional deflection due to the presence of the creep zone can be estimated using Irvin's concept of effective crack length, a_{eff}[20]

$$a_{eff} = a + \beta r_c \quad [7]$$

where a is physical crack length, r_c is the creep zone, and β is a scaling parameter. Since the creep zone can sustain stresses to certain extent, the entire creep zone does not act as a crack. Therefore, the value of β is less than one. If we choose the value of r_c corresponding to $\theta = 90$ deg, it has been shown that $\beta = 1/3$.[20] As the alloy develops damage zone ahead of the crack tip for both microstructural conditions,[21] effective crack length as mentioned previously has been used for analysis.

III. RESULTS AND DISCUSSION

The variation of LLD and crack length with time corresponding to $\alpha + \beta$ and β conditions at 600 °C is shown in Figures 2 and 3, respectively. The variation of LLD as well as crack length with time exhibit three well defined stages, *i.e.*, I, II, and III, similar to primary, secondary, and tertiary stages observed in creep curves.

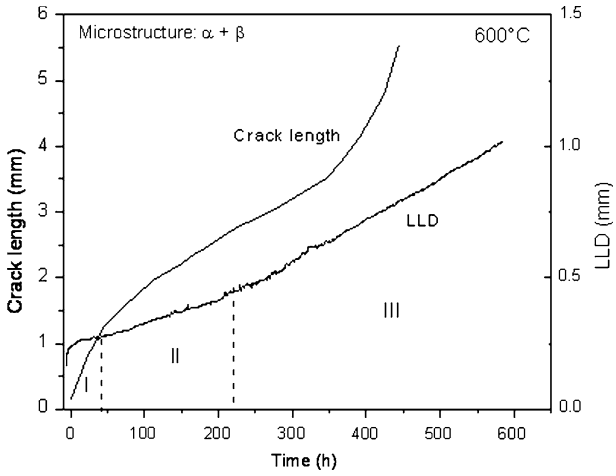

Fig. 2—Variation of crack length and LLD with time for the alloy with $\alpha + \beta$ microstructure at 600 °C.

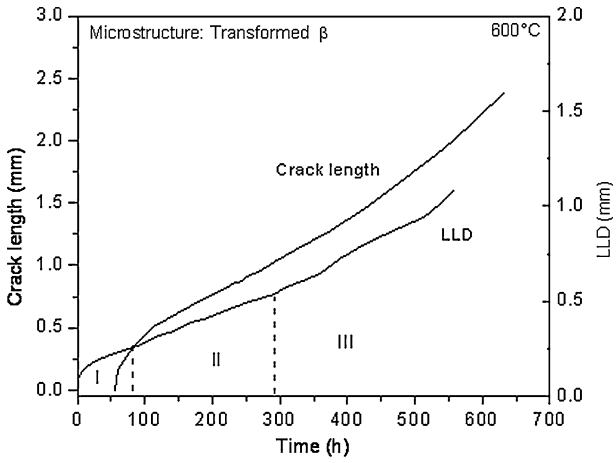

Fig. 3—Variation of crack length and LLD with time for the alloy with transformed β microstructure at 600 °C.

Stage I could be essentially attributed to large stress relaxation occurring at the crack tip, while stage II represents steady-state crack growth, and stage III is characterized by fast crack growth. Similar trends were observed for the CCG data at 550 °C for both microstructural conditions. It has been observed that CCG takes place largely during steady-state condition. While no incubation period for the crack initiation was observed for all test conditions investigated in $\alpha + \beta$ condition, the alloy in the β treated condition exhibited incubation periods of 8 hours and 56 hours for test temperatures 550 °C and 600 °C, respectively. The reasons for existence of incubation periods for CCG in case of transformed β structure are not clear at this stage.

A. *Choice of Crack-tip Parameter*

1. *Stress intensity parameter (K)*

The titanium alloys have been reported[13,15] to exhibit either creep-brittle or creep-ductile behavior depending upon microstructure and test temperature. As a first

choice, due to its simple definition, the stress intensity parameter K, widely used for creep-brittle materials such as nickel base superalloys,[11,12] has been chosen to characterize CCG behavior of the present alloy. The variation of the creep crack growth rate (CCGR) da/dt with the stress intensity factor K on log-log scale for the alloy in both $\alpha + \beta$ and β conditions at 600 °C are shown in Figures 4(a) and (b), respectively. Crack growth rate initially decreases with increase in K (pretransition regime), then starts increasing linearly beyond certain K level (post-transition regime). The CCGR data corresponding to the post-transition regime follows a power-law equation of the form

$$\frac{da}{dt} = A(K)^m \qquad [8]$$

where $\frac{da}{dt}$ is the CCGR, K the stress intensity factor, and A and m are material constants (Table I). The CCG data corresponding to post-transition region are consolidated for all test conditions in Figure 5. The general observation is that bimodal $\alpha + \beta$ microstructure exhibits higher exponent, m (~7 and 17) than β microstructure (~2 and 3.5) at both test temperatures (Table I). Further, for both microstructures the CCG curves are observed to be steeper at 550 °C than those at 600 °C, the effect being more pronounced for $\alpha + \beta$ microstructure. It could be further observed that the alloy with β microstructure exhibits better CCG resistance than the alloy with $\alpha + \beta$ microstructure.

Although the stress intensity factor K is able to describe CCGR data well in post-transition regime, its validity to characterize CCG appears to be questionable in the present case due to several reasons. First, the validity of K parameter requires satisfying a minimum

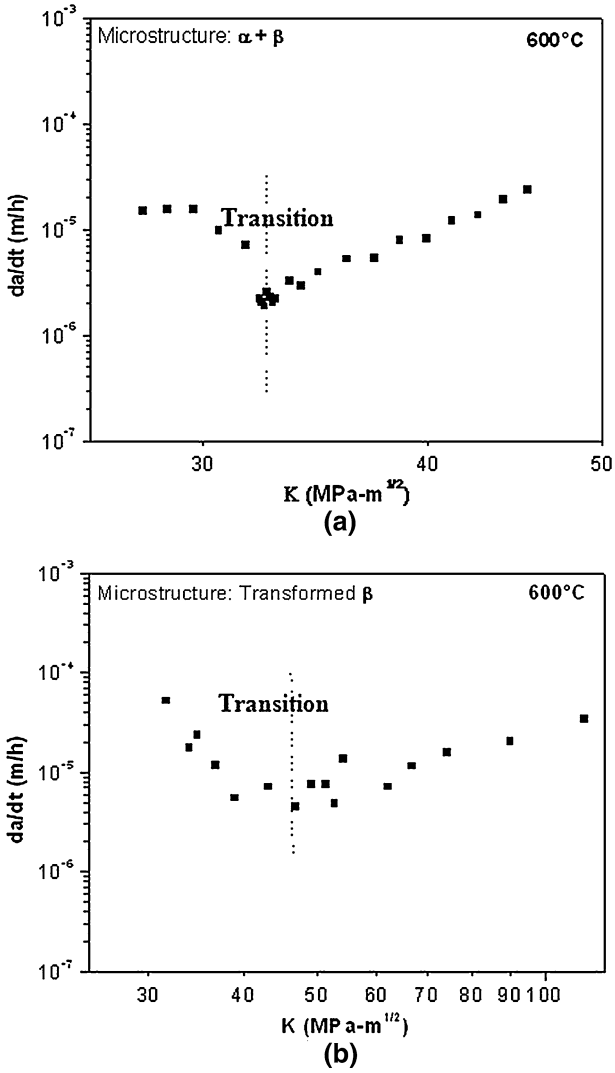

Fig. 4—(*a*) Variation of crack growth rate with stress intensity factor K for $\alpha + \beta$. (*b*) Variation of crack growth rate with stress intensity factor K for transformed β microstructures.

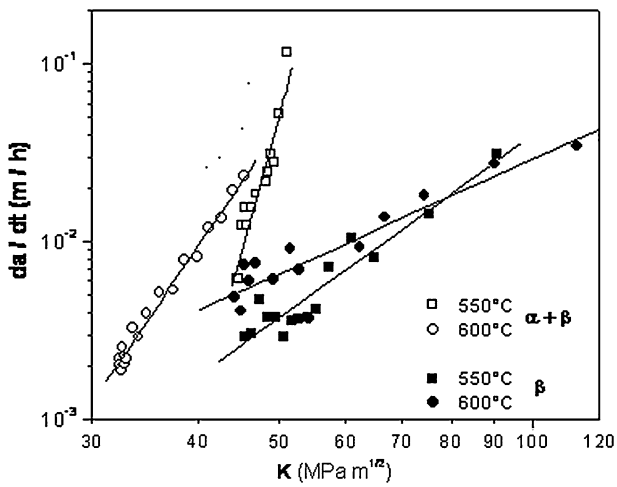

Fig. 5—Variation of crack growth rate with stress intensity factor K of the alloy in both $\alpha + \beta$ and transformed β microstructural conditions.

Table I. Creep Crack Growth Constants

	Test Temperature (°C)							
	550 °C				600 °C			
Microstructure	A	m	B	r	A	m	B	r
Bimodal ($\alpha + \beta$)	2.9×10^{-31}	~17	2.39×10^{-32}	~45	5.9×10^{-14}	~7	4.47×10^{-8}	8.7
Transformed β	6.1×10^{-9}	3.5	9.5×10^{-13}	~12	2.2×10^{-6}	~2	1.78×10^{-6}	~5

Note: $da/dt = A(K)^m$; $da/dt = B(C_t)^r$.

test specimen thickness criteria for prevalence of plane strain conditions per ASTM E-399-90 standard:[18]

$$B \geq 2.5(K/\sigma_{ys})^2 \qquad [9]$$

where B is the thickness of the specimen and σ_{ys} yield strength of the material. The thickness value calculated for 600 °C at $K = 25$ MPa$\sqrt{\text{m}}$ is ~9 mm, which is much higher than the specimen thickness (~2 mm) used in the present investigation. In the present case, the CCG data has been generated over a wide range (K ~ 25 to 90 MPa$\sqrt{\text{m}}$), the K becomes inappropriate under all test conditions. Second, the K parameter does not take into account stress relaxation occurring at the crack tip due to extensive creep deformation as evident from the LLD plots (Figures 2 through 4). Hence, attempts have been made to identify other parameters that could capture these effects in their formulation.

The pretransition regime (Figure 4) exhibiting an anomalous behavior, *i.e.*, decreasing crack growth rate with increasing K, has been reported for creep-ductile[14] and creep-brittle[13] types of materials. In such cases, the creep-ductile materials have been best characterized by C_t or C^* parameters. Transients of this nature have been observed in creep-brittle materials if crack growth extension is preceded by an incubation period.[14] In such cases, a transient time t_g is defined, which is the time needed for crack to grow through the creep zone, which forms ahead of the crack tip during the incubation period.[14] Such a case has been best resolved by accounting effect of growing crack in estimating size of creep zone in calculation of C_t parameter. For time greater than t_g it has been shown that for creep-brittle materials, the CCGR can be correlated well with K.[14] Norris *et al.*[15] has reported similar behavior in damage tolerant titanium alloy 6222, which has been identified to exhibit such a dual slope behavior. It has been reported that at higher temperatures (400 °C to 450 °C), the alloy behaves as creep-ductile, whereas creep-brittle behavior remains dominant at lower temperature (350 °C). In light of this understanding, other parameters that account for this apparent anomaly in CCG have been investigated.

2. *Energy integral parameter (C_t)*

As per ASTM standard E-1457[2] for CCG testing, the precise choice of crack-tip parameter for characterizing CCGR has been based on the ratio of creep deflection rate $\dot{\upsilon}_c$ to the total deflection rate $\dot{\upsilon}$, *i.e.*, $\dot{\upsilon}_c/\dot{\upsilon}$. It has been established that creep-ductile behavior dominates for $\dot{\upsilon}_c/\dot{\upsilon}$ values ≥0.5 and path-independent energy rate line integral C^* parameter has been used to characterize CCG behavior in this case. On the other hand, for creep-brittle materials with $\dot{\upsilon}_c/\dot{\upsilon} \leq 0.5$, LEFM parameters K or J may be applicable. The variation of $\dot{\upsilon}_c/\dot{\upsilon}$ with time for the present IMI-834 titanium alloy for the two microstructural conditions is shown in Figure 6. It can be seen that the $\dot{\upsilon}_c/\dot{\upsilon}$ values, which are quite high (~0.9) initially, are observed to decrease with crack growth and remain consistently higher than ~0.5 until termination stage. Further, β microstructure exhibits higher $\dot{\upsilon}_c/\dot{\upsilon}$ values than those of $\alpha + \beta$ microstructure. The higher values of

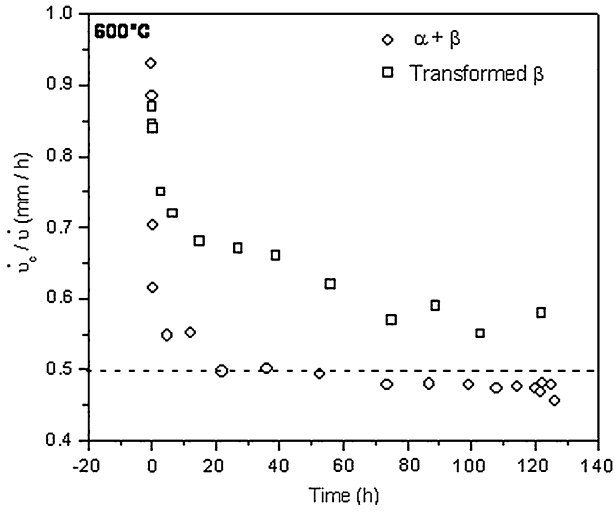

Fig. 6—Variation of $\dot{\upsilon}_c/\dot{\upsilon}$ with time for the alloy in $\alpha + \beta$ and transformed β microstructural conditions.

$\dot{\upsilon}_c/\dot{\upsilon}$ (≥0.5) suggest that the alloy exhibits creep-ductile behavior in the temperature range 550 °C to 600 °C. Hence, C^* or C_t could be used to characterize the CCG behavior of this alloy. In addition, the higher creep ductility of ~20 pct observed in the temperature range of investigation in conventional creep deformation tests[22] further fortifies the argument that the present titanium alloy system could be categorized as a creep-ductile material as per ASTM standard E-1457[2] and under such conditions C^* or C_t is an obvious field parameter for CCG characterization. As mentioned in Section II–C, applicability of C^* is only limited to extensive steady-state creep conditions and does not take into account SSC conditions as manifested by pretransition regime exhibiting anomalous behavior of decreasing crack growth rates with increasing K. Hence, the C_t parameter is considered as crack-tip parameter in the present investigation to characterize the creep crack behavior.

The variation of the CCGR with the parameter C_t for the alloy in both $\alpha + \beta$ and β conditions is shown in Figure 7. The data for different heat treatment and test conditions were fit according to a power-law equation of the form

$$da/dt = B(C_t)^r \qquad [10]$$

where B and r are the material constants, and their values under various conditions are given in Table I. The trends of these plots are the same as those characterized by da/dt *vs* K plots for post-transition regime (Figure 5). The CCG exponent (r) values corresponding to bimodal microstructure are much higher (~9 and 45) than those for β microstructure (~5 and 12) for both test temperatures. Further, it is observed that these values are higher at 550 °C than those at 600 °C for both the microstructures. It could be further inferred that the alloy with fully transformed β structure has better CCG resistance than that with bimodal microstructure at both temperatures, *i.e.*, 550 °C and 600 °C. This observation is consistent with the creep behavior

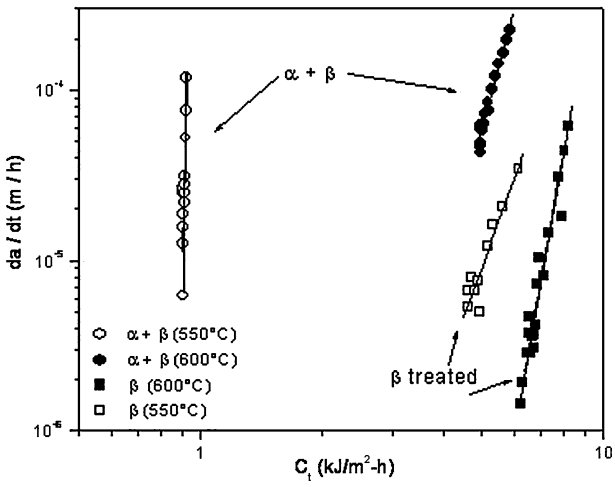

Fig. 7—Variation of crack growth rate with energy integral parameter C_t of the alloy in both $\alpha + \beta$ and transformed β microstructural conditions.

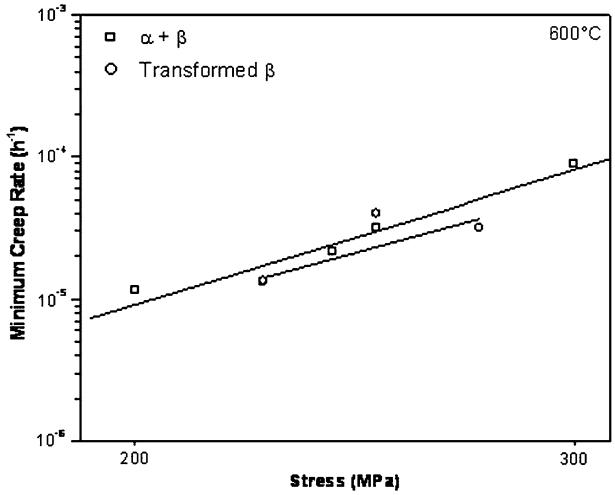

Fig. 8—Variation of minimum creep rate with stress at 600 °C.

observed for these two microstructural conditions on conventional smooth creep deformation specimens, *i.e.*, the alloy with transformed β microstructure exhibits better creep resistance than that with bimodal microstructure, as shown in Figure 8. Only limited studies on effect of microstructure on CCG behavior of titanium alloy have been reported in literature. Dogan *et al.*[13] have investigated Ti-6242 titanium alloy exhibiting creep-brittle behavior and reported that bimodal (microstructure exhibited lower CCGRs (*i.e.*, higher CCG resistance) than that of β microstructure. This trend was observed to be reversed if creep resistance based on smooth specimen creep test data of the two microstructures are compared, *i.e.*, β microstructure showed superior creep resistance than bimodal microstructure. The observed lower creep resistance of the bimodal microstructure as compared to the fully transformed β structure has been attributed to the alloying element partitioning effect that reduces the strength of the

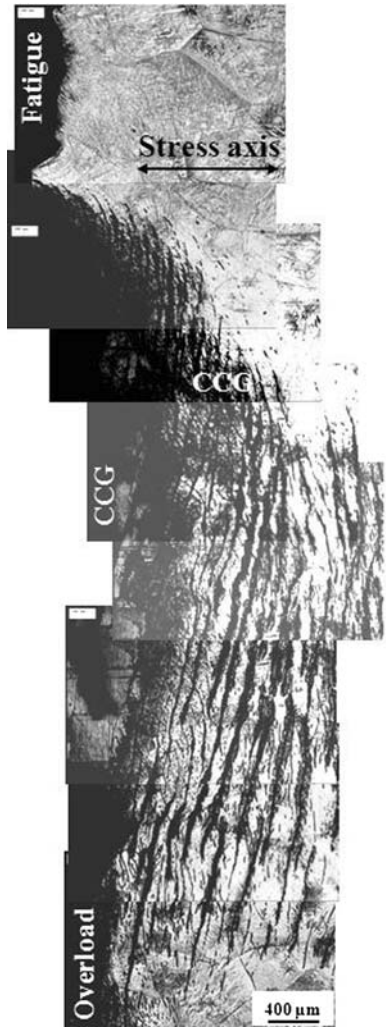

Fig. 9—Series of optical micrographs of the in-plane cross section of a CCG specimen for the transformed β microstructure tested at 600 °C.

lamellar matrix of the bimodal in comparison to the fully lamellar microstructure.[19]

B. *Effect of Microstructure on CCG Micromechanisms*

1. *Creep crack path profile and fracture morphology*

Figure 9 shows a series of overlapping optical micrographs illustrating a typical crack path profile of CCG specimen tested at 600 °C in β treated condition. A number of secondary surface cracks almost parallel to the main crack (*i.e.*, perpendicular to stress direction) are evident from this composite micrograph. Similar behavior has also been observed in case of the alloy with $\alpha + \beta$ microstructure. The fractographic features of the CCG tested specimens at 600 °C are shown in Figures 10 and 11 for transformed β microstructure. Figure 10(a) shows macrofeatures of the entire fracture surface of the specimen depicting various regions including machine notch, fatigue precrack, creep crack, and overload fracture regions. The fatigue precrack zone in Figure 10(b) shows transgranular features with

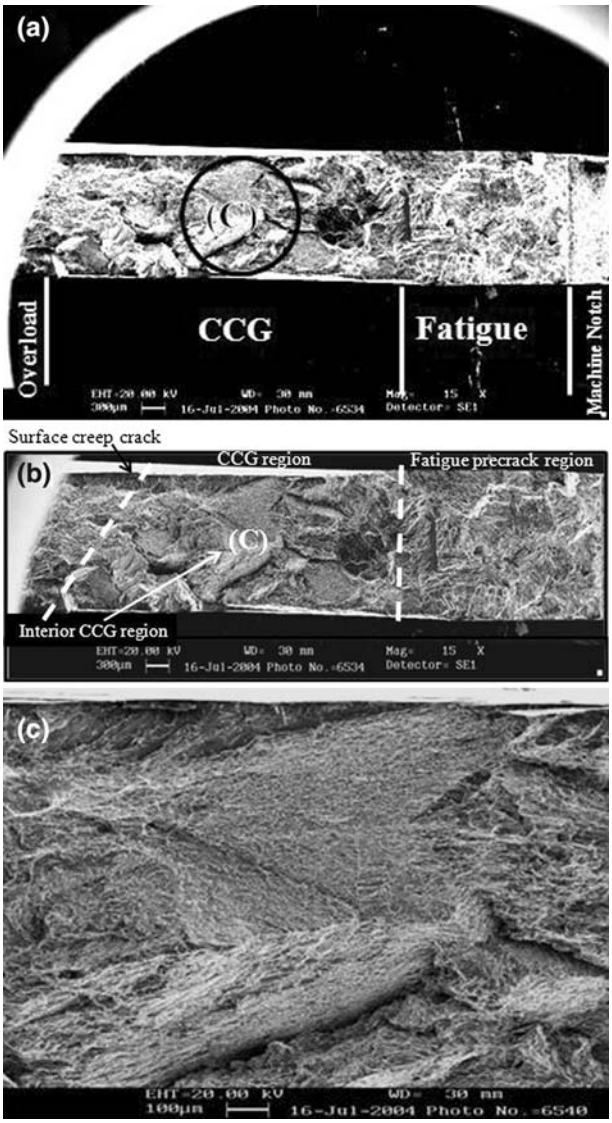

Fig. 10—(*a*) Fracture surfaces of the creep crack growth tested specimen at 600 °C for transformed β microstructure, (*b*) various creep crack growth regions, and (*c*) creep crack zone depicting intergranular dimples on grain facets.

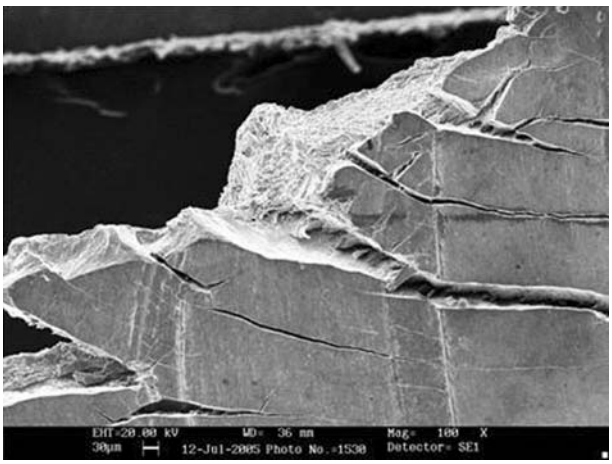

Fig. 11—Fractograph showing penetration of surface cracks in transformed β microstructure.

fracture occurring across both the primary α particles as well as transformed β laths. While fracture surface in CCG region as illustrated in Figure 10(b) exhibits two regions, *viz*., external region close to surface formed by penetration of environment assisted surface creep cracks (Figure 11) from either side across the specimen thickness. The interior CCG region shows (Figure 10(b)) mixed mode fracture features of intergranular facets and transgranular dimples with former being more predominant. A magnified view of this region reveals intergranular dimples on grain facets (Figure 10(c)). On the other hand, the interior CCG region in case of the alloy with $\alpha + \beta$ microstructure exhibits predominantly dimple features, suggesting that fracture was caused by nucleation, growth, and coalescence of microvoids in $\alpha + \beta$ microstructure.

2. *CCG mechanisms*

One important observation common to both microstructures is that there are a number of secondary surface cracks (perpendicular to the stress axis) formed around the main crack, thus suggesting that CCG is associated with formation of damage zone ahead of the crack tip (Figures 9 and 12). Micrographs shown in Figures 12 through 16 illustrate microscopic aspects of CCG in β and $\alpha + \beta$ microstructures. Detailed fractographic

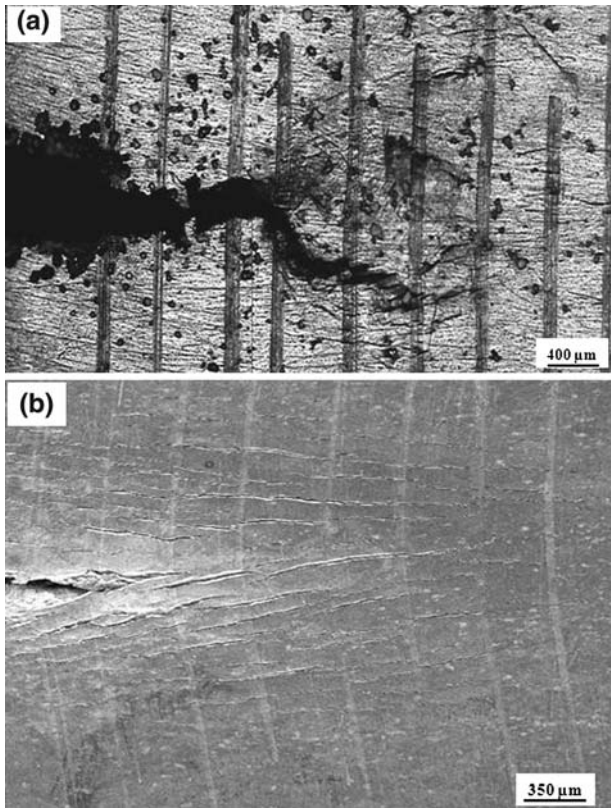

Fig. 12—(*a*) Microscopic aspects of the CCG of the alloy (interrupted during early stages of CCG) in β. Figure reveals nucleation of cavities at titanium-rich oxide particles formed around crack tip. (*b*) Microscopic aspects of the CCG of the alloy (interrupted during early stages of CCG) in $\alpha + \beta$. Figure illustrates formation of a number of surface cracks parallel to the main crack.

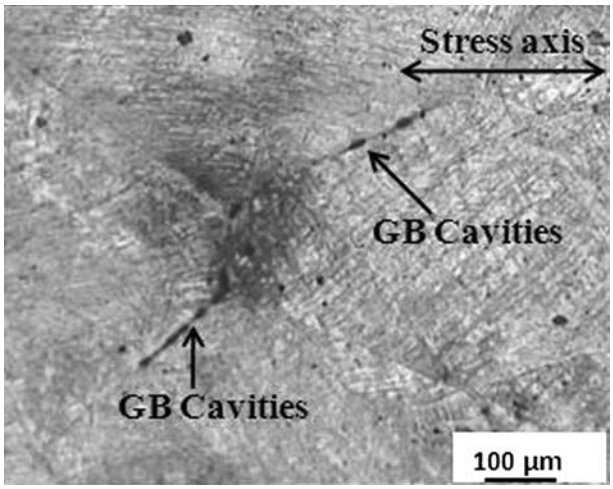

Fig. 13—Optical micrograph showing cavities on grain boundaries (inclined/normal to the stress axis) in the interior CCG region of the alloy with transformed β structure at 600 °C.

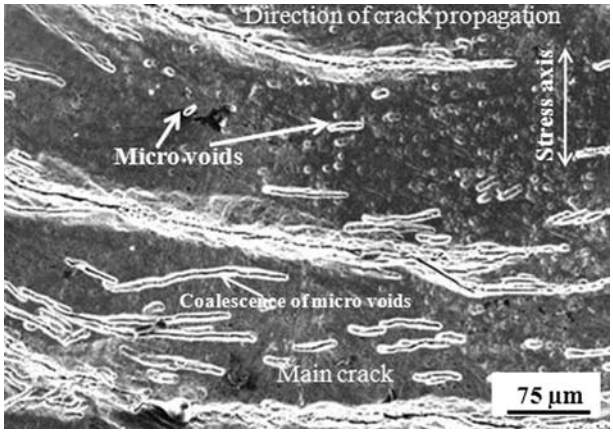

Fig. 14—Microstructure on surface of the specimen revealing various stages such as nucleation and coalescence of microvoids close to the crack tip.

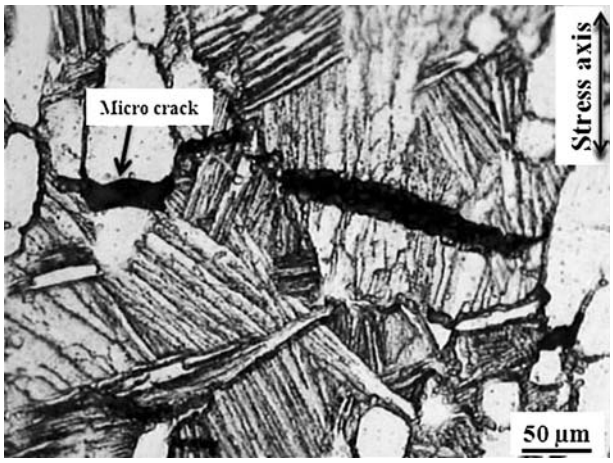

Fig. 15—Formation and linkage of microcracks at the primary α particles.

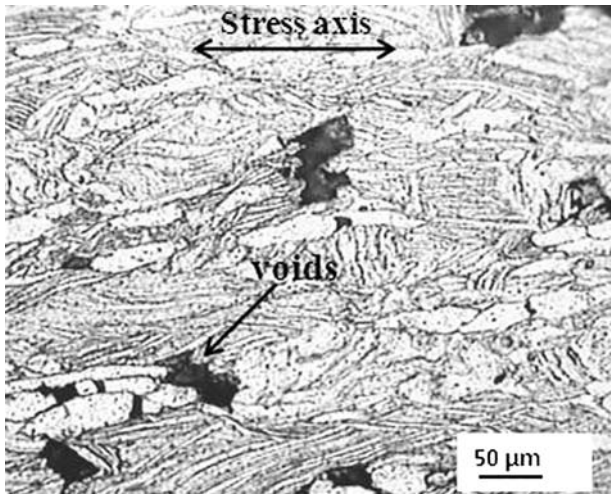

Fig. 16—Optical micrograph showing microvoids at primary α/transformed β interface in the interior CCG region of the alloy with $\alpha + \beta$ microstructure at 600 °C.

and microstructural examination of damage zone has revealed that the CCG in stable crack growth regime comprises two stages, *viz*., (1) nucleation of microvoids/microcracks around crack tip and (2) growth and coalescence of microvoids/microcracks, which subsequently join the main crack. The details of CCG mechanisms for both types of microstructure are discussed in the subsequent sections.

a. β microstructure. While the exterior region of fracture surface in CCG region shows transgranular dimples, the interior region exhibits intergranular dimples (Figure 10(c)). Similar features are also observed in case of smooth creep specimens with transformed β structure.[22] As evident from the micrograph shown in Figure 12(a), the damage at the surface accumulates in the form of cavities within the transformed β regions, and a number of vertical lines seen in Figures 12(a) and (b) are lines inscribed on specimen to optically confirm crack length with ACPD technique. These cavities were found to nucleate at second phase particles (Figure 12(a)), which were identified as titanium-enriched oxide by energy-dispersive X-ray analysis in scanning electron microscopy. The size of these oxide particles varies from less than 1 μm to as high as 50 μm. It is observed that voids are nucleated essentially by particle decohesion (Figure 12(a)). On the other hand, in the interior regions of the specimen, cavities have formed at grain boundaries, which are inclined/normal to the stress axis (Figure 13). These features were revealed by polishing into the specimen interior close to fracture end. This observation is in line with creep studies performed on smooth creep specimens with transformed β microstructure.[22] In both the cases, the cavities grow in the creeping matrix around crack tip with continued creep deformation. Creep data on smooth specimens has indicated that the alloy in both β microstructure and bimodal microstructure deforms by power-law creep.[22,23] On this basis, it is appropriate

to expect that the alloy in the creep zone, *i.e.*, close to and little ahead of the crack tip deforms according to a power-law relationship. This suggests that the growth of voids nucleated in this zone is controlled by the power-law creep of the surrounding regions. Once these voids grow to sufficient size, the adjacent voids coalesce to produce microcracks. The microstructure in the surface region shown in Figure 14 reveals all stages, such as nucleation of microvoids, coalescence of microvoids leading to formation of microcracks, and linking up of microcracks. The micrograph in Figure 14 illustrates the microstructure close to the crack tip in the polished condition. It is to be noted that the coalescence of microvoids and their subsequent linking up take place in the direction perpendicular to the applied stress axis. It is observed that the microcracks propagate across α laths. It is clearly evident from this microstructure that the cracks are essentially propagating perpendicular to the stress axis and not following any specific path, such as lath interfaces or prior β grain boundaries. Further careful examination of microstructure close to the crack tip has indicated two possible ways as to how growth and coalescence of voids nucleated at oxide particles assist surface CCG in this alloy. In the first case, the crack grows by joining of the voids nucleated with the main crack tip. Alternatively, a secondary crack forms ahead of the crack tip by growth and coalescence of voids and eventually joins the main crack to cause creep crack extension.

The important point to be noted is that although numerous surface cracks have formed due to environmental interaction, the penetration of these microcracks into the specimen interior, as evident from Figures 10 and 11, has been limited to a thickness of ~200 μm from either surface of the specimen.

b. $\alpha + \beta$ microstructure. In contrast to the observations in the alloy in β microstructure, where microvoids nucleated at the surface oxide particles, microcracks have been found to form by fracture of primary α particles at the specimen surface in bimodal microstructure (Figure 15). This may be due to the well-documented fact that α phase has more affinity as well as solid solubility for oxygen. The dissolution of oxygen in the α phase during CCG test makes the latter brittle, and as a result, microcrack nucleation takes place during the creep deformation by fracture of primary α particles. Figure 15 illustrates the nucleation of microcracks at primary α particles and subsequent linkage of these microcracks. A number of secondary cracks have also formed in the region all around the main crack tip and ahead of it. On the other hand, cavities or voids have formed at primary α/transformed β structure (*i.e.*, matrix) interface in the interior CCG region of the specimen (Figure 16) as also observed in smooth creep specimens with ($\alpha + \beta$) microstructure.[22] The growth of both surface microcracks and interior microvoids is controlled by creep of the surrounding region.

Despite the differences in initiation of fracture at nucleation stage (microvoids/microcracks) for these two microstructural conditions, the CCG in both cases is controlled by creep deformation of the surrounding regions. Since the alloy with fully transformed β structure exhibits better creep resistance, CCG rates are lower for transformed β microstructure.

IV. CONCLUSIONS

1. The applicability of stress intensity factor K is not appropriate in the present study due to stress relaxation at the crack tip and specimen thickness invalidity as per linear elastic fracture mechanics requirement.
2. The C_t parameter for both microstructural conditions correlates well with CCGR data and is well described by a power law of the form $\left(\frac{da}{dt}\right) = B(C_t)^r$.
3. For all test conditions investigated, the alloy with transformed β microstructure exhibits superior CCG resistance to that with $\alpha + \beta$ microstructure. This observation is consistent with the better creep resistance of the alloy with transformed β microstructure.
4. Creep crack growth for both microstructural conditions is accompanied by formation of damage zone in the form of numerous environmental-assisted secondary surface cracks (perpendicular to the stress axis) ahead of the main crack tip.
5. For $\alpha + \beta$ microstructure of the alloy, the surface creep cracks were formed by growth and coalescence of microcracks nucleated by fracture of primary α particles. In the interior of the specimens CCG occurred by growth and coalescence of microvoids nucleated at primary α/transformed β (matrix) interfaces.
6. For β microstructure of the alloy, the surface creep cracks formed by growth and coalescence of microvoids nucleated at titanium-enriched surface oxide particles, while in the interior CCG occurred by nucleation of intergranular cavities.

ACKNOWLEDGMENTS

The authors are grateful to the DRDO for the financial assistance received. They acknowledge Mr. B. Narsing Rao, S.M. Gupta, and Raja Rao for their help at various stages of investigation. The authors express their gratitude to Dr. G. Malakondaiah, Director, DMRL, for timely suggestions and constant encouragement at all stages of work.

REFERENCES

1. G. Nagalakshmi and V. Kumar: DMRL TR 2005371, DMRL, Hyderabad, 2005.
2. *Standard Test Method for Measurement of Creep Crack Growth Rates in Metals*, ASTM E 1457-00, ASTM, Philadelphia, PA, vol. 03.01, 1995, pp. 960–74.
3. *Evaluation of C_t Parameter for Characterizing CCGR in the Transient Regime*, ASTM STP 905, John L. Bassani, Donald E. Hawk, and Ashok Saxena, eds., ASTM, Philadelphia, PA, 1989, pp. 7–26.

4. *Evaluation of C* for the Characterizing of Creep-Crack-Growth Behavior in 304 Stainless Steel*, ASTM STP 700, A. Saxena, ed., ASTM, Philadelphia, PA, 1980, pp. 131–51.
5. A. Saxena, H.A. Ernst, and J.D. Landes: *Int. J. Fract.*, 1983, vol. 23, pp. 245–57.
6. H. Riedel and V. Detampel: *Int. J. Fract.*, 1987, vol. 33, pp. 239–62.
7. K.M. Nikbin: *Int. J. Press. Vess. Pip.*, 2003, vol. 80 (7–8), pp. 415–16.
8. K. Sadanada and P. Shahinian: *Eng. Fract. Mech.*, 1981, vol. 15 (3–4), pp. 327–40.
9. S.H. Ryu, Jinyu, and S.H. Hong: *Metall. Mater. Trans. A*, 1997, vol. 28A, pp. 629–34.
10. T. Hollsteir and B. Voss: ASTM STP 995, ASTM, Philadelphia, PA, pp. 195–213.
11. S. Xu, A.K. Koul, and J.I. Dickson: *Metall. Mater. Trans. A*, 2001, vol. 32A, pp. 795–804.
12. M. Tabuchi, K. Kabu, K. Yagi, A.T. Yokobori, and A. Fuji: *Eng. Fract. Mech.*, 1999, vol. 62, pp. 47–60.
13. B. Dogan, A. Saxena, and K.H. Schwalbe: *Mater. High Temp.*, 1992, vol. 10 (2), pp. 138–43.
14. B. Dogan and K.H. Schwalbe, *Creep Crack Growth Behavior of Titanium Alloy, Fracture Mechanics: 22nd Symp.*, ASTM STP 1131, H.A. Ernst, A. Saxena, and D.L. McDowell, eds., ASTM, Philadelphia, PA, 1992, vol. I, pp. 284–96.
15. R.H. Norris, A. Saxena, and J. Tucker: *Eng. Fract. Mech.*, 1999, vol. 62, pp. 79–97.
16. A. Saxena: *Non-Linear Fracture Mechanics for Engineers*, CRC Press, Boca Raton, FL, 1998, pp. 309–62.
17. Y. Murakami: *Handbook of Stress Intensity Factors*, Pergamon Press, Headington Hill Hall, Oxford, England, 1987, vol. 1, pp. 9–10.
18. H. Riedel and J.R. Rice: *Fracture Mechanics: 12th Conf*, ASTM STP 700, ASTM, Philadelphia, PA, 1980, pp. 112–30.
19. K. Ohji, K. Ogura, and S. Kubo: *JSME*, 1979, No. 790-13, pp. 18–20 (in Japanese).
20. A. Saxena: *Eng. Fract. Mech.*, 1991, vol. 40, pp. 721–36.
21. J.L. Bassani, D.E. Hawk, and A. Saxena: *Non-Linear Fracture Mechanics: Time Dependent Fracture Mechanics*, ASTM, STP 995, Philadelphia, PA, 1989, vol. I, pp. 7–29.
22. D.V.V. Satyanarayana, T. Sridhar, B. Narsingh Rao, G.B. Vikram, Ch. Swarnakumari, and Vikas Kumar: DMRL TR 2005380, DMRL, Hyderabad, Aug. 2005.
23. M.Es. Souni: *Mater. Charact.*, 2001, vol. 46, pp. 365–79.